Accepted for publication in The Astrophysical Journal
Preprint typeset using LaTeX style emulateapj v. 10/09/06

THE INTEGRATED POLARIZATION OF SPIRAL GALAXY DISKS

Jeroen M. Stil
Centre for Radio Astronomy, University of Calgary

Marita Krause and Rainer Beck
Max Planck Institut für Radio Astronomie, Auf dem Hügel, Bonn, Germany

A. Russell Taylor
Centre for Radio Astronomy, University of Calgary

Draft version October 13, 2008

ABSTRACT

We present integrated polarization properties of nearby spiral galaxies at 4.8 GHz, and models for the integrated polarization of spiral galaxy disks as a function of inclination. Spiral galaxies in our sample have observed integrated fractional polarization in the range $\lesssim 1\%$ to 17.6%. At inclinations less than 50 degrees, the fractional polarization depends mostly on the ratio of random to regular magnetic field strength. At higher inclinations, Faraday depolarization associated with the regular magnetic field becomes more important. The observed degree of polarization is lower ($< 4\%$) for more luminous galaxies, in particular those with $L_{4.8} > 2 \times 10^{21}$ W Hz^{-1}. The polarization angle of the integrated emission is aligned with the apparent minor axis of the disk for galaxies without a bar. In our axially symmetric models, the polarization angle of the integrated emission is independent of wavelength. Simulated distributions of fractional polarization for randomly oriented spiral galaxies at 4.8 GHz and 1.4 GHz are presented. We conclude that polarization measurements, e.g. with the SKA, of unresolved spiral galaxies allow statistical studies of the magnetic field in disk galaxies using large samples in the local universe and at high redshift. As these galaxies behave as idealized background sources without internal Faraday rotation, they can be used to detect large-scale magnetic fields in the intergalactic medium.

Subject headings: galaxies: magnetic fields — galaxies: spiral — radio continuum: galaxies — polarization

1. INTRODUCTION

Large-scale regular magnetic fields have been detected by Faraday rotation of radiation of polarized background sources in the Milky Way (Han et al. 1999; Brown et al. 2003, 2007), and the nearest galaxies (Stepanov et al. 2008; Arshakian et al. 2007), such as M31 (Han et al. 1998), and the Large Magellanic Cloud (Gaensler et al. 2005). The limiting factor for this work is the number density of bright polarized background sources. A few galaxies in the Local Group (M31, LMC) have angular sizes large enough to probe their magnetic field structure by rotation measures of polarized background sources with current radio telescopes. Magnetic fields in galaxies outside the Local Group have been studied mainly with imaging polarimetry at radio wavelengths (Beck 2005 for a review). These observations indicate a large-scale azimuthal magnetic field in the plane of the disk of spiral galaxies, normally oriented in a spiral pattern with a pitch angle similar to the optical spiral arms. High degrees of polarization have been observed in interarm regions of some galaxies, such as NGC 6946 (Beck 2007b). If a magnetic field is observed in a barred galaxy, it is aligned with the bar inside the region of the bar, with a spiral pattern outside the bar region (Beck et al. 2002). However, some barred galaxies show no detectable polarized emission or polarized emission along the bar.

Statistical information on magnetic fields in galaxies is required to study the cosmic evolution of these magnetic fields by observing galaxies over a range of redshift. Polarimetric imaging of a large sample of spiral galaxies in the local universe is impractical with current instrumentation because of the high sensitivity and angular resolution required. On the other hand, deep polarization surveys of the sky are underway or being planned that will have the sensitivity to detect spiral galaxies out to large distances, but not resolve these galaxies. The first deep wide-area polarimetry survey with the sensitivity to detect spiral galaxies is GALFACTS[1] at 1.4 GHz, 5σ point source sensitivity of 400μJy, and resolution $3'$. SKA pathfinder telescopes such as ASKAP (Johnston et al. 2007) aim to do all-sky polarimetry surveys at 1.4 GHz with an instantaneous band width of 300 MHz with thousands of spectral channels and a 5σ point source sensitivity around 50 μJy (Johnston et al. 2007). ASKAP will be able to detect a few thousand spiral galaxies at sufficient signal to noise ratio to detect polarization at the few percent level, but the expected angular resolution of $8''$ to $\sim 1'$ will not resolve these galaxies. This raises the question what can be learned about magnetic fields from polarimetry of large samples of unresolved spiral galaxies.

Observations of polarization from spiral galaxies at redshifts up to 1 or higher will require the Square Kilometre Array[2] (SKA), and even then it will be diffi-

[1] http://www.ucalgary.ca/ras/GALFACTS
[2] http://www.skatelescope.org

cult to make resolved polarization maps of these high-redshift galaxies. The origin and evolution of cosmic magnetism is one of five key science drivers for the SKA (Gaensler et al. 2004). For the evolution of magnetic fields in spiral galaxies as a function of redshift, polarization of the integrated emission is most readily observable, and a comparison with unresolved galaxies at low redshift is relatively straightforward.

The number density of faint polarized radio sources in the sky determines the unknown confusion limit in polarization, and is an important parameter for rotation measure studies. Below 1 mJy total flux density, star forming galaxies become an increasingly important fraction of all radio sources. Knowledge of the polarization properties of these galaxies is required to make realistic predictions of the number of polarized sources at μJy levels in polarized flux density. Spiral galaxies may become an important fraction of the polarized 1.4 GHz radio source population at μJy flux densities (Stil et al. 2007).

This paper presents observations and models that show that unresolved spiral galaxies have detectable polarized emission, sometimes more than 10% polarized at 4.8 GHz, and that statistical information on magnetic fields and internal Faraday rotation can be derived from integrated polarization measurements of spiral galaxies.

2. OBSERVATIONS

We use a compilation of archival data for nearby galaxies imaged in polarized radio emission. Observations at 4.8 GHz are most widely available, so this paper focuses at this frequency to maximize the sample size for a single frequency. Additional observations at 8.4 GHz are available for five galaxies. These are listed alongside the 4.8 GHz data. Three sub samples are distinguished in this paper. The first sub sample is a set of 14 nearby "field" galaxies listed in Table 1. The second sub sample is a set of 9 spiral galaxies in the Virgo cluster from Weżgowiec et al. (2007), Weżgowiec et al. (in prep.), and Chyży et al. (2007) listed in Table 2. These galaxies exist in a cluster environment, with a higher probability of interaction with other cluster members and the intracluster gas. The third sub sample of 20 barred spiral galaxies listed in Table 3 allows us to explore the integrated polarization of barred galaxies. One nearby galaxy (NGC 4631, classified as SB) was included in Table 3.

The nearest galaxies in the sample and the galaxies in the Virgo cluster were observed with the 100m-Effelsberg telescope, sometimes in combination with the VLA. These galaxies are not affected by missing short spacings in the interferometer. The barred galaxies were not observed with the Effelsberg telescope, and the images could in principle lack large scale structure resolved by the shortest baselines of the interferometer. A comparison of 6 cm flux densities derived by Beck et al. (2002) with published integrated flux densities showed that NGC 1313 and NGC 3992 in Table 3 may be affected by missing short spacings, because published flux densities listed in the NASA Extragalactic Database (NED) are substantially higher than the 6-cm flux density in Beck et al. (2002). If no 6 cm flux density was published, we compared the 21 cm flux density corrected for a spectral index 0.7 - 1 with the flux density in Beck et al. (2002). Of the two barred galaxies with suspected missing flux in the interferometer image, NGC 1313 showed no significant integrated polarization, while NGC 3992 has a high degree of polarization of 14.9 ± 4.8 %. Most of the emission of NGC 3992 detected in the interferometer image originates outside the bar region (Beck et al. 2002).

In order to simulate unresolved observations from our maps of nearby galaxies we integrated the Stokes I, Q, and U images of these galaxies separately in ellipses. Their axial ratio was defined by the outer isophotes in the Stokes I image and the ellipses include the entire galaxy up to the noise level of the Stokes I map. The integrated Q and U flux densities were used to calculate the integrated polarized flux density $S_p = \sqrt{(Q^2 + U^2)}$, that was corrected for polarization bias following Simmons & Stewart (1985) to obtain the intrinsic polarized flux density $S_{p,0}$. The correction for polarization bias did not have a measurable effect for most galaxies because of the high signal to noise ratio of the integrated flux densities. The integrated fractional polarization of each galaxy was calculated as $\Pi_0 = S_{p,0}/S$, where S is the total flux density, including thermal and non-thermal emission. The polarization angle $\theta_{\rm pol} = \frac{1}{2}\arctan(U/Q)$ of the integrated emission is expected to be aligned with the apparent minor axis of the optical galaxy. The sensitivity of the observations is included in the errors for Π_0 through the noise in the maps. The error estimates also include the uncertainty in the zero level, that dominates the uncertainty for galaxies with a large angular size such as M 31. It is customary to list the position angle of the optical major axis, and also to rotate the observed E-vectors by 90° to obtain B-vectors in the plane of the sky. We therefore define $\theta_{\rm B} = \theta_{\rm pol} + 90°$ for comparison with published position angles of the optical major axis, $\theta_{\rm opt}$. The results are listed in Tables 1, 2, and 3.

Bandwidth depolarization is negligible in these data. For a rotation measure as high as 300 rad m^{-2}, the polarized intensity is decreased by less than 1%. The integrated polarized flux densities are not affected by significant residual instrumental polarization. Small values for the integrated fractional polarization are the result of integrating significant flux in Stokes Q and U, with nearly equal positive and negative contributions. The uncertainty in the polarization angle of the integrated emission is typically less than 5 degrees.

Some galaxies (M 31, M 81, NGC 4565 in Table 1, NGC 4192, NGC 4302, NGC 4535 in Table 2, NGC 1300, NGC 1493, NGC 3953, NGC 3992 in Table 3) have integrated fractional polarization $\Pi_0 > 7$%. Five of these galaxies (M 31, NGC 4565, NGC 4192, NGC 1493, and NGC 3992) are more than 10% polarized after integration over solid angle.

Five of the Virgo galaxies have additional observations at 8.4 GHz. The fractional polarization at both frequencies agrees to within a few percent for these galaxies. Small differences can be attributed to statistical errors, mainly at 8.4 GHz where the signal to noise ratio of the emission is lower. The differences in Π_0 at 4.8 GHz and at 8.4 GHz per galaxy are much smaller than the differences between galaxies. This confirms that the variation in Π_0 between galaxies represents intrinsic differences between the galaxies. The polarization angles at 4.8 GHz and

TABLE 1
Integrated polarization of nearby spiral galaxies

Source	Type	i (°)	ν (GHz)	S_ν (mJy)	S_ν(10 Mpc)[a] (mJy)	Π_0 (%)	θ_B (°)	θ_{opt} (°)	Tel.[b]
IC 342	SAB(rs)cd	25	4.8	856	82	2.2 ± 0.1	50 ± 1	39	E
M 31	SA(s)b	76	4.8	1863	9	17.6 ± 3.5	68 ± 4	38	E
M 33	SA(s)cd	56	4.8	1539	11	1.4 ± 0.4	77 ± 6	23	E
M 51	SAbc	20	4.8	380	358	2.8 ± 0.3	−46 ± 2	−10	E+V
M 81	SA(s)ab	59	4.8	385	41	7.3 ± 0.3	−36 ± 1	−28	E
M 83	SAB(s)c	24	4.8	809	111	2.5 ± 0.4	9 ± 4	45	E+V
NGC 253	SAB(s)c	78	4.8	2707	82	1.9 ± 0.2	51 ± 2	52	E+V
NGC 891	SA(s)b? sp	88	4.8	286	264	1.6 ± 0.1	6 ± 1	23	E
NGC 3628	SAb pec sp	89	4.8	247	111	4.0 ± 0.1	105 ± 1	104	E
NGC 4565	SA(s)b? sp	86	4.8	54	85	10.5 ± 0.3	−43 ± 1	−44	E
NGC 4736	(R)SAB(rs)ab	35	4.8	125	27	2.4 ± 0.4	−86 ± 3	−65	E+V
NGC 5775	SAbc	81	4.8	94	670	0.5 ± 0.2	−31 ± 9	−35	V
NGC 5907	Sc	87	4.8	72	87	2.2 ± 0.3	−6 ± 3	−25	E
NGC 6946	SAB(rs)cd	38	4.8	457	224	1.5 ± 0.5	−82 ± 7	60	E+V

[a] Flux density scaled to a distance of 10 Mpc.[b] Imaging telescope: E = Effelsberg 100m; E+V = Effelsberg 100m combined with the Very Large Array(VLA). References: IC 342: Gräve & Beck (1988), M 31: Berkhuijsen et al. (2003), M 33: Tabatabaei et al. (2007), M 51: Fletcher et al. (2004), M 81: Beck et al. (1985), M 83: Beck (2007a) from Beck, Ehle & Sukumar (unpubl.), NGC 253: Heesen et al. (2008), NGC 891, NGC 3628, and NGC 4565: Dumke & Krause (1998), NGC 4736: Chyży & Buta (2008), NGC 5775: Tüllmann et al. (2000), NGC 5907: Dumke et al. (2000), NGC 6946: Beck & Hoernes (1996); Beck (2007b)

TABLE 2
Integrated polarization of Virgo galaxies

Source	Type	i (°)	ν (GHz)	S_ν (mJy)	Π_0 (%)	θ_B (°)	θ_{opt} (°)	Tel.[a]
NGC 4192	SABb	78	8.4	16	14.5 ± 1.0	−28 ± 1	−27	E
			4.8	38	11.9 ± 0.5	−21 ± 1		E
NGC 4254	SA(s)c	42	4.8	167	1.4 ± 0.1	−46 ± 1	68	E+V
NGC 4302	SAc	90	8.4	22	5.8 ± 1.0	−13 ± 4	−2	E
			4.8	36	8.4 ± 0.7	−8 ± 1		E
NGC 4303	SABbc	18	8.4	107	1.5 ± 0.3	−13 ± 4	−28	E
			4.8	189	0.7 ± 0.1	−65 ± 4		E
NGC 4321	SAB	30	8.4	66	2.3 ± 0.4	−58 ± 4	−60	E
			4.8	109	1.0 ± 0.2	−52 ± 4		E
NGC 4388	SAb	82	4.8	74	1.1 ± 0.1	−60 ± 3	−89	E
NGC 4501	SAb	61	4.8	115	1.0 ± 0.1	−27 ± 3	−42	E
NGC 4535	SABc	44	8.4	20	6.7 ± 1.1	17 ± 3	0	E
			4.8	38	8.0 ± 0.4	15 ± 1		E
NGC 4654	SABc	56	4.8	51	3.3 ± 0.2	−47 ± 1	−59	E

[a] Imaging telescope: E = Effelsberg 100m; E+V = Effelsberg 100m combined with the Very Large Array(VLA). References: NGC 4192, NGC4302, NGC4303: unpublished images courtesy M. Weżgowiec and M. Urbanik, NGC 4254: Chyży et al. (2007), NGC 4388, NGC 4501, NGC 4535, and NGC 4654: Weżgowiec et al. (2007).

8.4 GHz are also mutually consistent. In low-inclination galaxies, the polarization angle of the integrated emission is more affected by asymmetries because the effect of an axially symmetric component on the polarization vanishes mostly. This can explain the difference in polarization angle for NGC 4303 ($i = 18°$). The position angle of the major axis can also be affected by ellipticity of the disk.

The fractional polarization of any particular galaxy depends on the direction from which the galaxy is observed, as the projection of the magnetic field on the plane of the sky and the path length of the line of sight through the disk change. Any particular galaxy can only be observed from one direction, but the variation of integrated polarization properties with inclination can be revealed for a sufficiently large sample of galaxies. The wide range in inclination ($20° < i < 90°$) in the sample allows an effective analysis of the integrated polarization properties of spiral galaxies as a function of inclination. It should be noted that the sample is not randomly distributed in inclination. The galaxies in Tables 1, 2, and 3 were observed to study their magnetic field configuration through imaging polarimetry. The sample is biased towards low inclination (face-on) and high-inclination (edge-on) galaxies because these were preferred for imaging of the magnetic field. In particular, the sub sample of barred spirals in Table 3 contains only galaxies with inclination $i < 60°$, with the exception of the added nearby galaxy NGC 4631. Any sample of spiral galaxies with inclination derived from the apparent axial ratio appears deficient in galaxies with $i \lesssim 20°$ because the disks of most spiral galaxies are not exactly circular (Binney & de Vaucouleurs 1981; Grosbøl 1985; Lambas et al. 1992). This effect is also apparent in the present sample, but it does not affect our analysis.

Figure 1 shows Π_0 as a function of inclination. The

TABLE 3
Integrated polarization of barred galaxies

Source	Type	i (°)	ν (GHz)	S_ν (mJy)	S_ν(10 Mpc) (mJy)	Π_0^a (%)	θ_B (°)	θ_{opt} (°)	Tel.[b]
NGC 1097	SBbc(rs)	45	4.8	155	397	(0.7 ± 0.8)	...	−45	V
NGC 1300	SBb(s)	35	4.8	10	38	7.6 ± 2.0	89 ± 6	86	V
NGC 1313	SBc(s)	38	4.8	22	4	(0.7 ± 1.3)	...	−10	A
NGC 1365	SBb(s)	40	4.8	205	740	(0.3 ± 0.2)	...	40	V
NGC 1433	SBb(s)	27	4.8	2	3	(4.7 ± 3.1)	...	17	A
NGC 1493	SBc(rs)	30	4.8	2	3	13.6 ± 3.5	29 ± 5	...[c]	A
NGC 1559	SBc(s)	55	4.8	105	235	1.9 ± 0.1	−50 ± 1	−115	A
NGC 1672	SBb(rs)	39	4.8	105	236	1.5 ± 0.2	−55 ± 3	−10	A
NGC 2336	SBbc(r)	59	4.8	4	35	(3.6 ± 3.5)	...	−2	V
NGC 2442	SBbc(rs)	24	4.8	71	182	1.1 ± 0.5	51 ± 9	40	A
NGC 3059	SBc(s)	27	4.8	29	56	(0.8 ± 0.5)	...	...[c]	A
NGC 3359	SBc(s)	55	4.8	13	29	(0.7 ± 1.4)	...	−10	V
NGC 3953	SBbc(r)	61	4.8	6	14	8.5 ± 2.7	50 ± 6	13	V
NGC 3992	SBb(rs)	59	4.8	4	8	14.9 ± 4.8	25 ± 7	67	V
NGC 4535	SBc(s)	26	4.8	12	30	6.4 ± 1.4	8 ± 4	28	V
NGC 4631	SB(s)d	85	4.8	476	268	1.1 ± 0.1	16 ± 2	86	E
NGC 5068	SBc(s)	29	4.8	14	7	(1.8 ± 1.6)	...	−20	V
NGC 5643	SBc(s)	30	4.8	59	116	1.0 ± 0.2	−68 ± 4	...[c]	A
NGC 7479	SBbc(s)	45	4.8	32	365	3.9 ± 0.6	−9 ± 3	25	V
NGC 7552	SBbc(s)	31	4.8	110	485	1.2 ± 0.2	−87 ± 4	1	A

[a] Galaxies with Π_0 less than 2 times the formal error listed in parentheses; these galaxies are not included in figures[b] Imaging telescope: A = Autralia Telescope Compact Array (ATCA), E = Effelsberg 100 m, V = VLA.[c] Position angle of major axis undetermined for this low-inclination galaxy. References: NGC 4631: Krause et al. (unpubl.) but see Krause (2003) and Golla & Hummel (1994); all other galaxies from Beck et al. (2002).

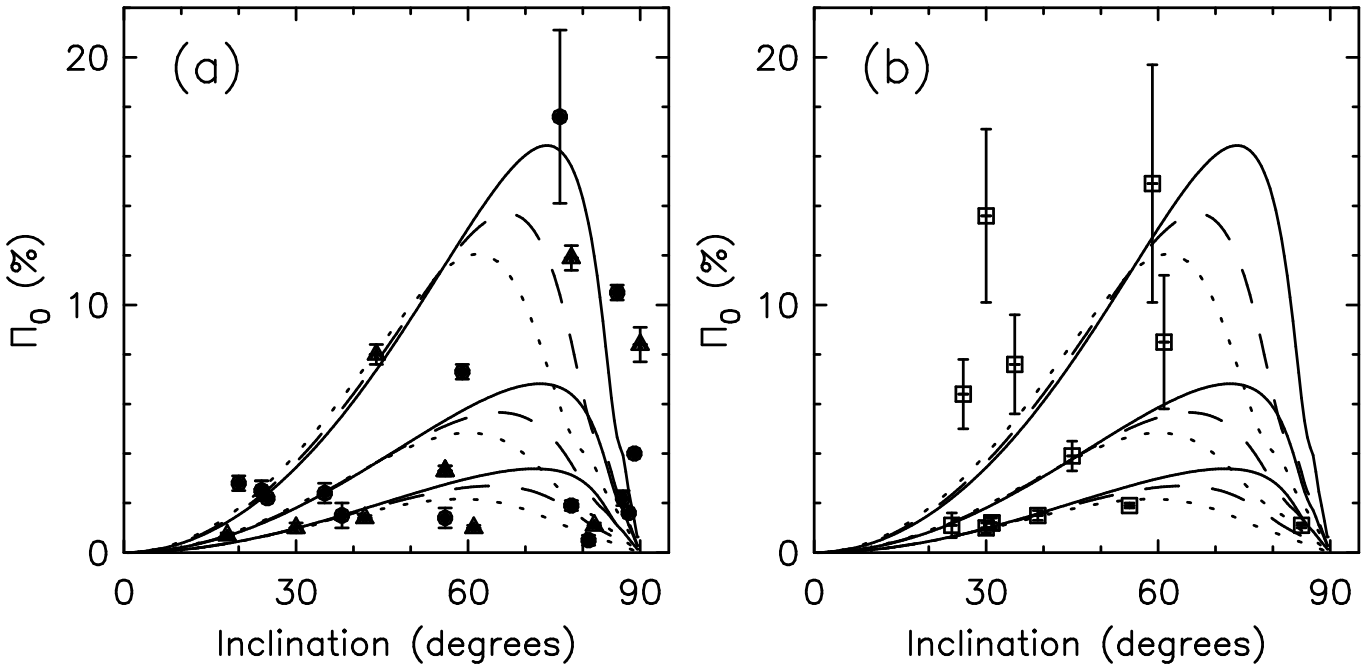

Fig. 1.— (a) Integrated fractional polarization at 4.8 GHz of nearby spiral galaxies from Table 1 (filled circles) and Virgo cluster spirals from Table 2 (triangles), with model curves described in Section 3. The model curves from top to bottom correspond with models 1–9 in Table 5, in that order. (b) The same as (a) for the detected barred galaxies from Table 3 (squares). The model curves in (b) are shown for reference only.

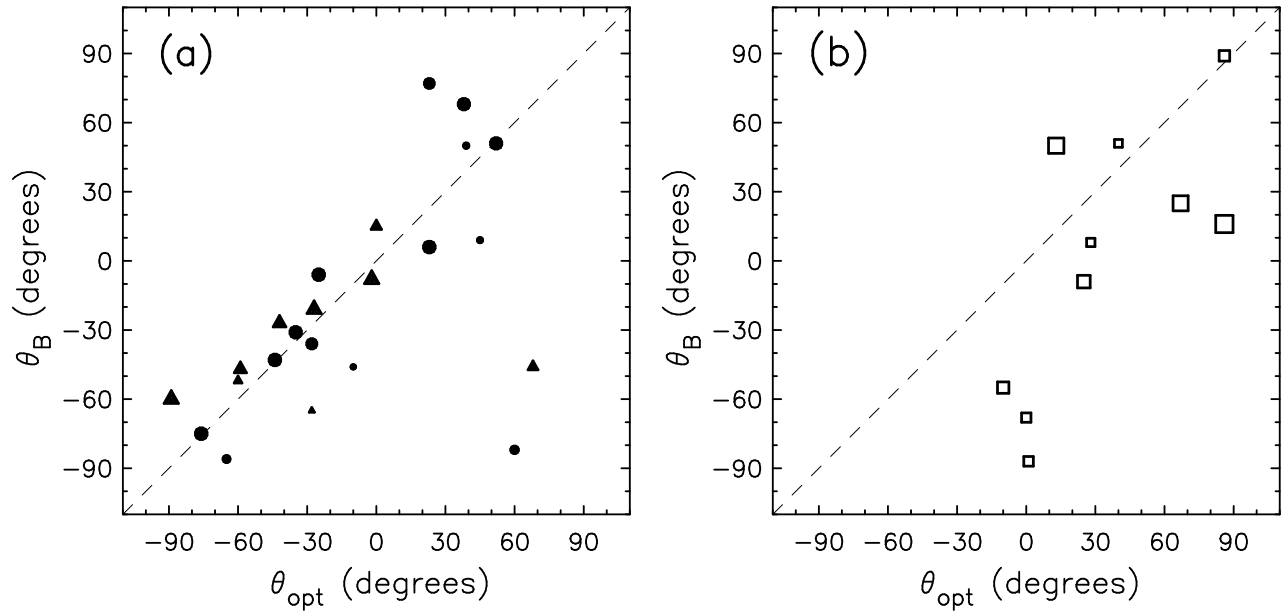

FIG. 2.— (a) Correlation between θ_{opt} and θ_B for galaxies in Table 1 (filled circles) and the Virgo galaxies in Table 2 (triangles). The symbol size increases linearly with $\sin(i)$. (b) The same as (a) for the barred galaxies in Table 3 (squares).

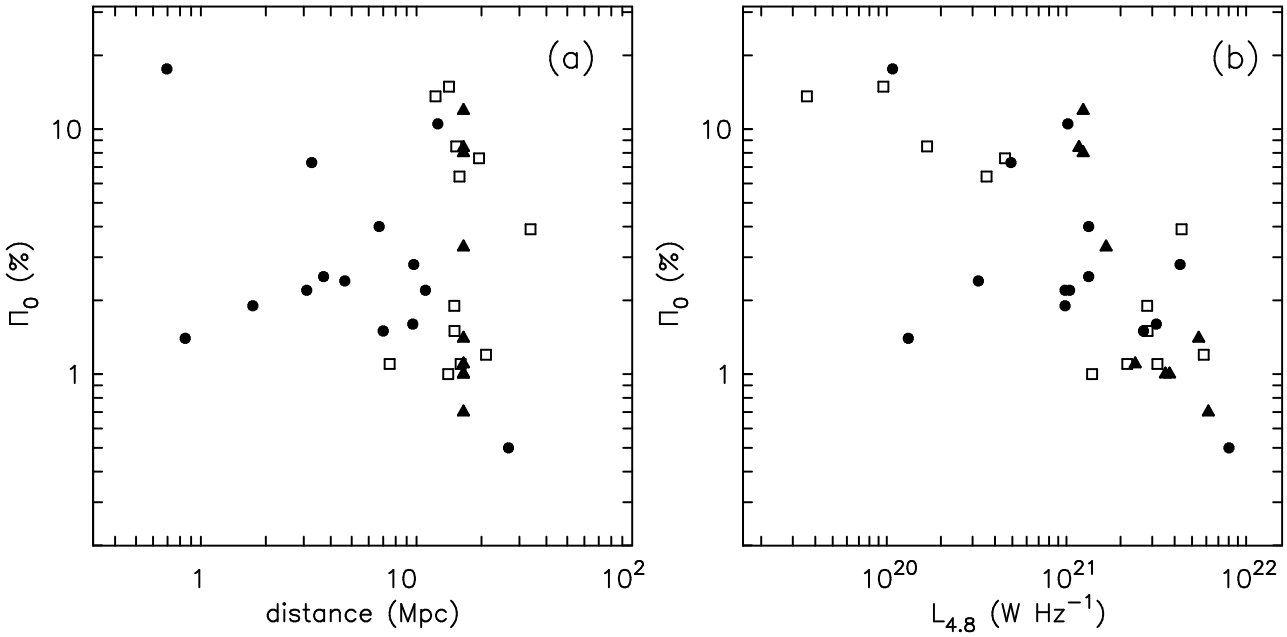

FIG. 3.— Integrated fractional polarization as a function of distance (a) and monochromatic 4.8 GHz luminosity (b) for the entire sample. The symbols are the same as in Figure 2. The symbols for the Virgo galaxies NGC 4321 and NGC 4501 overlap completely in (a), and partially in (b).

curves in Figure 1 represent models that will be discussed in Section 3. The formal errors on Π_0 are generally small because of the high signal to noise ratio in the integrated flux densities. Some galaxies with large angular size have larger errors because of uncertainties in the zero level of the maps. The large spread in Π_0, $1\% \lesssim \Pi_0 \lesssim 15\%$, seen for each subsample reflects intrinsic differences. The highest values of Π_0 in Figure 1a are found in the inclination range from $\sim 50°$ to $\sim 80°$. Some low-inclination galaxies with high Π_0 are found among the barred galaxies in Figure 1b. The model curves in Figure 1b are shown for reference only, as they do not include a bar.

Figure 2a shows the correlation between the position angle of the major axis, $\theta_{\rm opt}$, and $\theta_{\rm B}$ for galaxies in Table 1 and Table 2. If polarization of the integrated emission is the result of projection of the azimuthal magnetic field in the disk on the plane of the sky, a correlation is expected between $\theta_{\rm B}$ and the line of nodes of the disk intersecting the plane of the sky. The latter is determined by the position angle of the major axis, $\theta_{\rm B}$. The most deviating galaxies in Figure 2a are NGC 6946 and NGC 4254, with inclination $i = 38°$ and $i = 42°$ respectively. Large-scale departures from axial symmetry are most likely to be noticed for galaxies with a small inclination. The position angles used in Figure 2 are also less well defined. At lower inclinations, the position angle of the major axis is more difficult to measure because the isophotes are nearly circular. Besides measurement uncertainties, the position angle of the major axis is not a good estimator for the position angle of the line of nodes of the disk if the inclination approaches 26°, the inclination for which a circular disk would have an apparent axial ratio of 0.9, similar to the mean intrinsic ellipticity of spiral galaxy disks found by Lambas et al. (1992). Consequently, the uncertainty associated $\theta_{\rm opt}$ is substantial but hard to quantify for galaxies with inclination less than $\sim 40°$. For galaxies with higher inclinations, $\theta_{\rm opt}$ is estimated to be accurate to within $\sim 5°$. The uncertainty in $\theta_{\rm B}$ is typically a few degrees, but some additional scatter is expected because of differences in structure between galaxies. The total scatter in Figure 2a for galaxies with inclination $\gtrsim 60°$ suggests that the scatter introduced by structural differences is limited to $\pm 15°$.

Figure 2b shows the same relation for the detected barred galaxies in Table 3. The scatter between $\theta_{\rm opt}$ and $\theta_{\rm B}$ appears substantially larger than in Figure 2a. This may be a result of magnetic fields aligned with the bar, where the orientation of the bar adds a parameter to the problem. In this paper we focus mainly on galaxies without (strong) bars, while noting that unresolved barred galaxies can in fact also be polarized radio sources.

Figure 3 shows the integrated fractional polarization Π_0 as a function of distance, and monochromatic luminosity $L_{4.8}$. There should be no correlation between integrated polarization and distance, and none is found in the present sample. Figure 3b shows a correlation between Π_0 and $L_{4.8}$. There are no galaxies in the sample with $L_{4.8} > 2 \times 10^{21}$ W Hz^{-1} that have $\Pi_0 > 4\%$. Most galaxies with $L_{4.8} < 5 \times 10^{20}$ W Hz^{-1} do have $\Pi_0 > 4\%$. As shown in Figure 1, a galaxy can have low Π_0 because of strong Faraday depolarization, or because of its inclination. There is no correlation between inclination and luminosity in the sample. The lower integrated polarization of luminous galaxies in Figure 3b suggests stronger Faraday depolarization in these galaxies, or a lower degree of uniformity of the magnetic field as will be discussed in Section 4.1.

3. MODELS OF THE INTEGRATED POLARIZATION

3.1. *Polarized intensity in the disk*

The principal cause of net polarization of unresolved spiral galaxies is the regular azimuthal magnetic field in the disk projected on the sky along the apparent major axis. Faraday rotation and depolarization are affected by the path length through the disk, the line-of-sight component of the regular magnetic field, and fluctuations in thermal electron density and magnetic field strength. A first analysis of the integrated polarization of spiral galaxies is best served with the simplest possible model that includes these factors. We consider axially symmetric models with a regular azimuthal magnetic field in the disk, and an isotropic random component of the magnetic field.

Using this simple geometry, the integrated polarization of a spiral galaxy is modeled by considering each solid angle element of the disk as a slab with a specified line-of-sight component of the regular magnetic field that depends on inclination and location in the disk. Sokoloff et al. (1998) provided solutions of polarized intensity from a slab of Faraday-rotating medium mixed with relativistic electrons that produce synchrotron emission. The polarized intensity is expressed as a complex quantity $\mathcal{P} = Q + jU$ (Spangler 1982), where Q and U are Stokes parameters that describe the linear polarization. Following the conventions adopted by Sokoloff et al. (1998), $\mathcal{P}$, Q, and U are normalized by the total intensity of the synchrotron radiation, so that the modulus of $\mathcal{P}$ is the fractional polarization. The polarization angle of the complex polarization is $\Psi = \frac{1}{2}\arctan(U/Q)$.

At higher frequencies, a contribution from thermal emission to the total intensity reduces the observed fractional polarization by a factor $(1 - f_{th})$, where f_{th} is the fraction of the total intensity generated by thermal emission. We include thermal emission by setting $f_{th} = 0.23$ at 4.8 GHz (Condon & Yin 1990; Condon 1992; Niklas et al. 1997). Determination of f_{th} in individual galaxies is difficult because of the need to separate thermal and non-thermal emission in the radio spectrum. The rms scatter in f_{th} from galaxy to galaxy is believed to be at most a factor of 2 (Condon 1992). This translates into a spread of $\sim 25\%$ in $(1-f_{th})$ from the adopted value of 0.77.

In this paper we adopt a solution for the polarized intensity from a uniform slab of finite thickness along the line of sight from Sokoloff et al. (1998). For a given inclination i, the component of the regular magnetic field along the line of sight $B_\parallel$ and perpendicular to the line of sight $B_\perp$ can be evaluated. The uniformity of the magnetic field is expressed as the ratio of the isotropic random magnetic field strength to the regular magnetic field strength, defined as $f_B = \sigma_{\rm B}\sqrt{3}/B$, where $\sigma_{\rm B}$ is the rms strength of the random component of the magnetic field in one direction.

The complex polarization can be written as the product of a wavelength-independent part that describes the

TABLE 4
Sensitivity to model parameters[a]

Inclination	B	$f_{\rm B}$	n_e	f_i	$l_{\rm turb}$	$2h$
$i = 40°$	0.007	1.01	0.006	0.034	0.042	0.035
$i = 60°$	0.17	1.09	0.17	0.12	0.057	0.006
$i = 75°$	0.50	0.83	0.51	0.45	0.055	0.45

[a] Numbers listed are normalized contributions to the total scatter in a Monte Carlo simulation with 10000 realizations per inclination per parameter, where all parameters were drawn independently from a uniform distribution. Parameters with a small contribution to the total scatter are relatively unimportant. Parameter ranges adopted in this simulation: $1 < B < 10$ μG, $0.7 < f_{\rm B} < 4.0$, $0.01 < n_e < 0.1$ cm^{-3}, $0.1 < f_i < 1.0$, $10 < l_{turb} < 100$ pc, $200 < 2h < 2000$ pc.

polarization if Faraday rotation effects can be neglected, and a wavelength-dependent part that includes Faraday rotation effects. The wavelength-independent part of the complex polarization is

$$\langle \mathcal{P}_0 \rangle = p_i \frac{B_\perp^2}{B_\perp^2 + 2\sigma_{\rm B}^2} \exp\big[2j(\tfrac{1}{2}\pi + \arctan(B_y/B_x))\big], \quad (1)$$

where $p_i \approx 0.75$ is the intrinsic maximum polarization for synchrotron emission in a regular magnetic field, and B_x and B_y are the components of the regular magnetic field along two orthogonal axes in the plane of the sky. Equation 1 assumes a constant spectral index of -1 for the synchrotron emission of a galaxy. We define the $x-axis$ along the apparent major axis of the disk. The brackets $\langle\cdot\rangle$ indicate that the emission is averaged over a volume in the disk, that is sufficiently narrow to keep the regular magnetic field constant inside the volume, but extends along the line of sight through the disk. This is a reasonable approximation except for very high inclinations $i \gtrsim 80°$, where the azimuthal field must change along the line of sight, but only if the line of sight is near the major axis.

Equation 1 includes the effect of decreased polarization because of the presence of a random component of the magnetic field in the plane of the sky. Sokoloff et al. (1998) referred to this as wavelength-independent depolarization. The term beam depolarization is sometimes used in this situation, but this term is used also in case of wavelength-dependent Faraday effects. The plane of polarization is perpendicular to the component of the regular magnetic field projected on the plane of the sky.

The observed polarization $\langle \mathcal{P} \rangle$ differs from $\langle \mathcal{P}_0 \rangle$ because the polarized synchrotron emission generated in a small volume element in the disk is Faraday rotated as it travels through the disk to the observer. The effects of Faraday rotation can be written as a wavelength-dependent factor in the complex polarization, that includes an integral along the line of sight. Burn (1966) and Sokoloff et al. (1998) evaluated this integral analytically for a uniform slab. The observed polarized intensity from a small part of the disk is

$$\langle \mathcal{P} \rangle = \langle \mathcal{P}_0 \rangle \frac{1 - \exp(-S)}{S}, \quad (2)$$

where $S = 2\lambda^4 \sigma_{\rm RM}^2 - 2j\lambda^2 \mathcal{R}$ is a complex number that includes rotation measure fluctuations $\sigma_{\rm RM}$ in the real part and the Faraday depth $\mathcal{R}$ in the imaginary part.

The real part of S contains fluctuations in rotation measure along the line of sight through the factor $\sigma_{\rm RM}$,

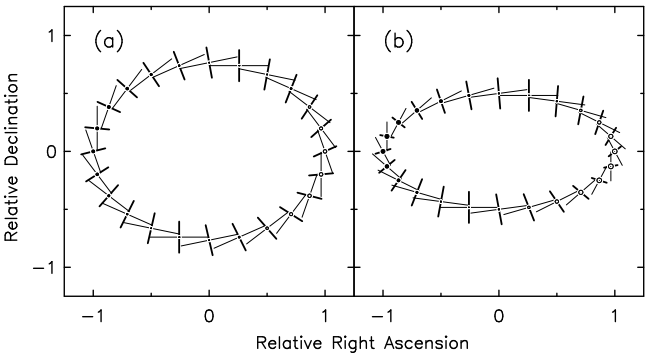

Fig. 4.— Representation of polarized intensity in an annulus of a spiral galaxy disk for $i = 40°$ (a), and $i = 60°$ (b). Thin lines represent the component of the magnetic field perpendicular to the line of sight, $B_\perp$. The pitch angle of the field is 15° in this example. Thick lines represent the polarization E-vectors, with length proportional to the polarized intensity. The line-of-sight component of the magnetic field $B_\parallel$ is indicated by open circles (towards the observer) and filled circles (away from the observer) with size proportional to $B_\parallel$. The integrated fractional polarization in (a) is $\Pi_0 = 6.1\%$, and in (b) $\Pi_0 = 13.1\%$, including a thermal fraction $f_{th} = 0.23$ at 4.8 GHz. The separation of the positions shown in this figure does not represent the step size of the integration.

which represents the rms amplitude of rotation measure fluctuations after integration along the line of sight. The plane of polarization makes a random walk because of fluctuations in density and magnetic field. When polarized emission is integrated over different lines of sight, or different depths inside the source, depolarization of the emission results. This process is called internal Faraday dispersion. Evaluation of $\sigma_{\rm RM}$ requires assumptions about the correlation scale of fluctuations in density and magnetic field strength. Sokoloff et al. (1998) discuss the difficulties estimating a correlation scale length, and assume that the scale length is the same for fluctuations in density, magnetic field, and rotation measure. The strength of the magnetic field in a turbulent cell defined by the correlation length is $\sigma_{\rm B}$. Rotation measure fluctuations also depend on the path length L through the disk with thickness $2h$, observed at inclination i, given by $L = 2h/\cos i$. The line-of-sight filling factor of the Faraday-rotating medium is f_i. Rotation measure fluctuations are then calculated following Sokoloff et al. (1998)

$$\sigma_{\rm RM} = 0.81 n_e \sigma_{\rm B} l_{\rm turb} \Big(\frac{2h f_i}{l_{\rm turb} \cos i} \Big)^{\frac{1}{2}} \quad (3)$$

The imaginary part of S describes rotation of the plane of polarization by the line-of-sight component of the regular magnetic field. The Faraday depth $\mathcal{R} = n_e f_i B_\parallel 2h/\cos i$ is the product of the mean electron density ($n_e f_i$), where n_e is the electron density in a turbulent cell, $B_\parallel$ the line-of-sight component of the regular magnetic field, and h the path length through the disk. Rotation of the plane of polarization also depolarizes emission integrated along the line of sight as emission from different depths of the source is rotated by different amounts. This mechanism for depolarization is called differential Faraday rotation. It is sometimes called depth depolarization, but it should be understood that there is a different depolarizing effect in the form of Faraday dispersion that is also the result of integrating emission along the line of sight.

3.2. *Integrated polarized emission*

TABLE 5
Model parameters for Figure 1

Model	B (μG)	$f_{\rm B}$	n_e (cm^{-3})	f_i	$l_{\rm turb}$ (pc)	$2h$ (pc)	f_{th}	$\Pi_{\rm max}$ (%)	$\Pi_{\rm med}$ (%)
1[a]	5.0	1.0	0.03	0.5	50	1000	0.23	16.4	10.2
2[b]	10.0	1.0	0.03	0.5	50	1000	0.23	13.7	8.2
3[c]	5.0	1.0	0.09	0.5	50	1000	0.23	12.0	7.0
4[a]	5.0	2.0	0.03	0.5	50	1000	0.23	6.8	4.7
5[b]	10.0	2.0	0.03	0.5	50	1000	0.23	5.6	3.7
6[c]	5.0	2.0	0.09	0.5	50	1000	0.23	4.8	3.1
7[a]	5.0	3.0	0.03	0.5	50	1000	0.23	3.4	2.4
8[b]	10.0	3.0	0.03	0.5	50	1000	0.23	2.7	1.8
9[c]	5.0	3.0	0.09	0.5	50	1000	0.23	2.2	1.4

[a] Models indicated by a solid curve in Figures 1 and 5[b] Models indicated by a dashed curve in Figures 1 and 5[c] Models indicated by a dotted curve in Figures 1 and 5

Equation 2 provides the complex polarized intensity $\langle\mathcal{P}\rangle$ for every line of sight, from which we obtain the local Stokes Q and U intensities, normalized by the local total intensity that is presumed uniform in the current models. The model Stokes Q and U intensities can be integrated over the disk to predict the model polarized flux density, fractional polarization Π_0, and the angle $\theta_{\rm B}$ of an unresolved spiral galaxy. The integration over the disk reduces to a one-dimensional numerical integration over azimuthal angle for the symmetric models under consideration.

Assuming values for the various model parameters, the integration over the disk can be performed as a function of inclination. The integrated polarization is more sensitive to certain model parameters, and the influence of model parameters can change with inclination. The relative importance of the parameters in our model was investigated through a Monte Carlo experiment. Each parameter was varied separately, and the resulting range of the integrated polarization was divided by the range obtained when all parameters were varied independently at the same time. The spread in integrated fractional polarization was taken as the difference between the upper quartile and the lower quartile. As the underlying distributions are strongly skewed, the quartiles provide a better indication of the spread in the distribution than the standard deviation. The normalization with the "total" scatter allows us to compare the importance of parameters between the three inclinations. It should be noted that the non-linear character of the model, and the opposing effects of certain parameters can make the ratio of the normalized quartile ranges larger than unity.

Table 4 shows for three values of the inclination the result of 10000 realizations of each parameter, drawn from a uniform distribution. The magnetic field strength, electron density, filling factor, turbulent length scale, and the vertical thickness of the disk were varied by an order of magnitude, as indicated in the footnote to Table 4. The ratio of random to regular magnetic field strength ($f_{\rm B}$) was varied over a smaller range (0.7 to 4.0). At low inclinations, the normalized quartile range for variation of $f_{\rm B}$ is 1.01, while the normalized quartile ranges of all other parameters are less than 0.1. Clearly, the ratio of random to regular magnetic field dominates the fractional polarization of the model for small inclinations. At $i = 60°$, $f_{\rm B}$ is still the most important parameter, but other parameters such as the regular magnetic field strength and the electron density become more important. At $i = 75°$, $f_{\rm B}$ is still important, but the parameters that define $\mathcal{R} = n_e f_i B_\parallel 2h/\cos i$ are almost equally important. The relative importance of n_e, f_i, B, and $2h$ is similar at $i = 75°$, because they contribute equally to $\mathcal{R}$, although subtle differences occur because of the dependence on $\sigma_{\rm RM}$. The turbulent scale length l_{turb} is the parameter in our model that is least constrained by observations. Table 4 shows that its effect on our results is insubstantial.

The simplest model is a disk with uniform parameters throughout that can be represented by a set of concentric annuli, all with the same integrated polarization properties. The model makes no assumptions about the magnetic field structure in the center of the disk. This is not a significant simplification for most spiral galaxies, where most of the polarized emission originates in the disk. Figure 4 shows a graphic representation of polarized intensity at a representative subset of locations (a ring) in the disk for model 1 in Table 5 at inclinations $i = 40°$ and $i = 60°$. Thin lines indicate the magnitude and direction of the magnetic field component in the plane of the sky, $B_\perp$. Thick lines represent polarization vectors. Open and filled circles represent the component of the regular magnetic field along the line of sight, $B_\parallel$.

At low inclination (Figure 4a), the path length through the disk is relatively small and the line-of-sight component of the regular field is also small. The polarized intensity in Figure 4a is fairly uniform across the disk and relatively high. At higher inclination, the path length through the disk increases, and the line-of-sight component of the regular magnetic field increases, in particular near the major axis. The polarized intensity is smaller everywhere in the disk, but most strongly near the major axis. Here, the line-of-sight component of the azimuthal regular field is largest, so Faraday rotation is strongest and the component $B_\perp$ (Equation 1) is smallest. Faraday depolarization is therefore strongest near the major axis, and the intrinsic polarization of the emission is smaller than elsewhere in the disk. Faraday rotation of the plane of polarization is also stronger near the major axis in Figure 4.

The model Stokes Q and U intensities, calculated by

solving Equation 2 for every line of sight through the disk, are integrated over the disk to predict the polarized intensity of an unresolved spiral galaxy. The integration over the disk reduces to a one-dimensional numerical integration over azimuthal angle for the symmetric models under consideration. The model in Figure 4a has integrated fractional polarization $\Pi_0 = 7.9\%$, while the model in Figure 4b has integrated fractional polarization $\Pi_0 = 17.0\%$. Despite the stronger depolarization anywhere in the disk at inclination $i = 60°$, the *integrated* polarization is stronger at $i = 60°$ than at $i = 40°$, because of the smaller degree of symmetry of the polarized emission.

The model predictions for Π_0 and θ_B are independent of the spiral pitch angle of the magnetic field. For a disk with constant thickness and uniform properties, the path length through the disk depends only on inclination, and the polarized intensity depends only on the angle of the regular component of the magnetic field with the line of sight. The effect of a pitch angle of the magnetic field, is to change the azimuthal angle in the disk where the line of sight makes a certain angle with the regular magnetic field. The integral over all azimuthal angles in the disk is not affected by a translation in azimuthal angle resulting from the pitch angle of the magnetic field.

Table 5 gives values for the parameters in the models that are compared with the data. Model 7 corresponds with the values adopted by Beck (2007b) for NGC 6946. The filling factor of ionized gas f_i and the thickness of the disk $2h$ were kept constant, because their effect on the models is similar to that of the electron density and the magnetic field. Model curves of fractional polarization as a function of inclination are shown in Figure 1. Three families of models are shown (Table 5), with $f_B = 1$, 2, and 3. For each value of f_B, model curves are shown for $n_e = 0.03$ cm^{-3}, $B = 5$ μG (solid curves), $n_e = 0.03$ cm^{-3}, $B = 10\mu$G (dashed curves), and $n_e = 0.09$ cm^{-3}, $B = 5$ μG (dotted curves).

At low inclination, the models are mainly distinguished by the value of f_B. The line-of-sight component of the regular magnetic field is small at low inclination, and the main depolarization mechanisms are wavelength independent depolarization and Faraday dispersion. At inclination $i \gtrsim 50°$, differential Faraday rotation along the line of sight becomes increasingly important, and significant effects of the strength of the regular magnetic field and the density of thermal electrons are found.

This effect already occurs at low inclination, where the line-of-sight component of the magnetic field near the major axis increases proportionally to i, but the path length through the disk $\sim 1/\cos i$ is constant to first order in i. The result is that models that include Faraday depolarization predict a *higher* degree of polarization at low inclinations than models that do not include Faraday depolarization (Stil et al. 2007). The present models also predict a higher fractional polarization at low inclination if the electron density n_e or the strength of the regular magnetic field is increased, if the ratio of random magnetic field to regular magnetic field strength is not too high.

The models more or less cover the same area of Figure 1a as the data. This result supports the idea that the observed integrated polarization of spiral galaxies is related to the large-scale field in the disk. The most notable difference between the data and the models is the observed low $\Pi_0 \lesssim 2\%$ of some galaxies with intermediate inclination, $40° \lesssim i \lesssim 60°$. It is difficult to change any single parameter in the model to obtain a fractional polarization $\Pi \lesssim 2\%$ in this inclination range, unless higher values of f_B are assumed.

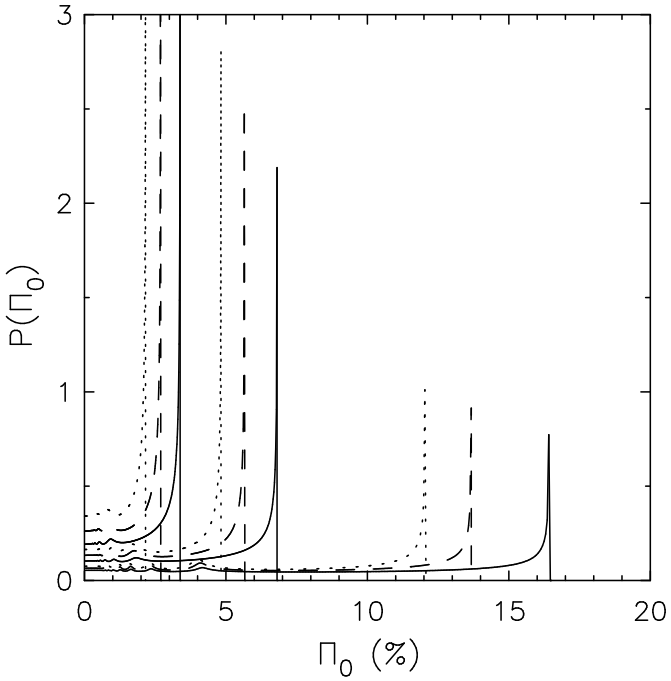

FIG. 5.— Probability density functions (PDF) of Π_0 for randomly-oriented spiral galaxies derived from the models in Figure 1. The continuous, dashed, and dotted curves correspond with models 1 – 9 in Table 5, in order of decreasing maximum Π_{max}. The curves are normalized such that the integral of the PDF is 1. Median values Π_{med} of these distributions are listed in Table 5.

3.3. *Probability distribution of* Π_0

The results in the previous sections suggest that the integrated 4.8 GHz emission of spiral galaxies can show substantial polarization. Deep polarization surveys can detect distant unresolved spiral galaxies. How many spiral galaxies can be detected, and the interpretation of unresolved galaxies detected in polarization, is determined by the probability density function (PDF) of the fractional polarization of spiral galaxies. The wavelength dependence of integrated polarization is also best summarized by means of the PDF of fractional polarization. In this section we discuss the expected shape of the PDF of fractional polarization for unresolved spiral galaxies at 4.8 GHz and 1.4 GHz. We also discuss the PDF of Π_0 in the special case of low-inclination galaxies ($i \lesssim 30°$), where the integrated polarization depends mostly on Faraday dispersion, but the actual value of the inclination cannot be determined reliably from the optical axial ratio.

The models for the integrated fractional polarization as a function of inclination can be used to derive a probability density function (PDF) for Π_0 of unresolved, randomly oriented spiral galaxies. This PDF can be used to predict the number of spiral galaxies detectable in deep polarization surveys based on population models of the total intensity source counts (Stil et al. 2007). The shape of the PDF can be modeled as a function of rest-frame

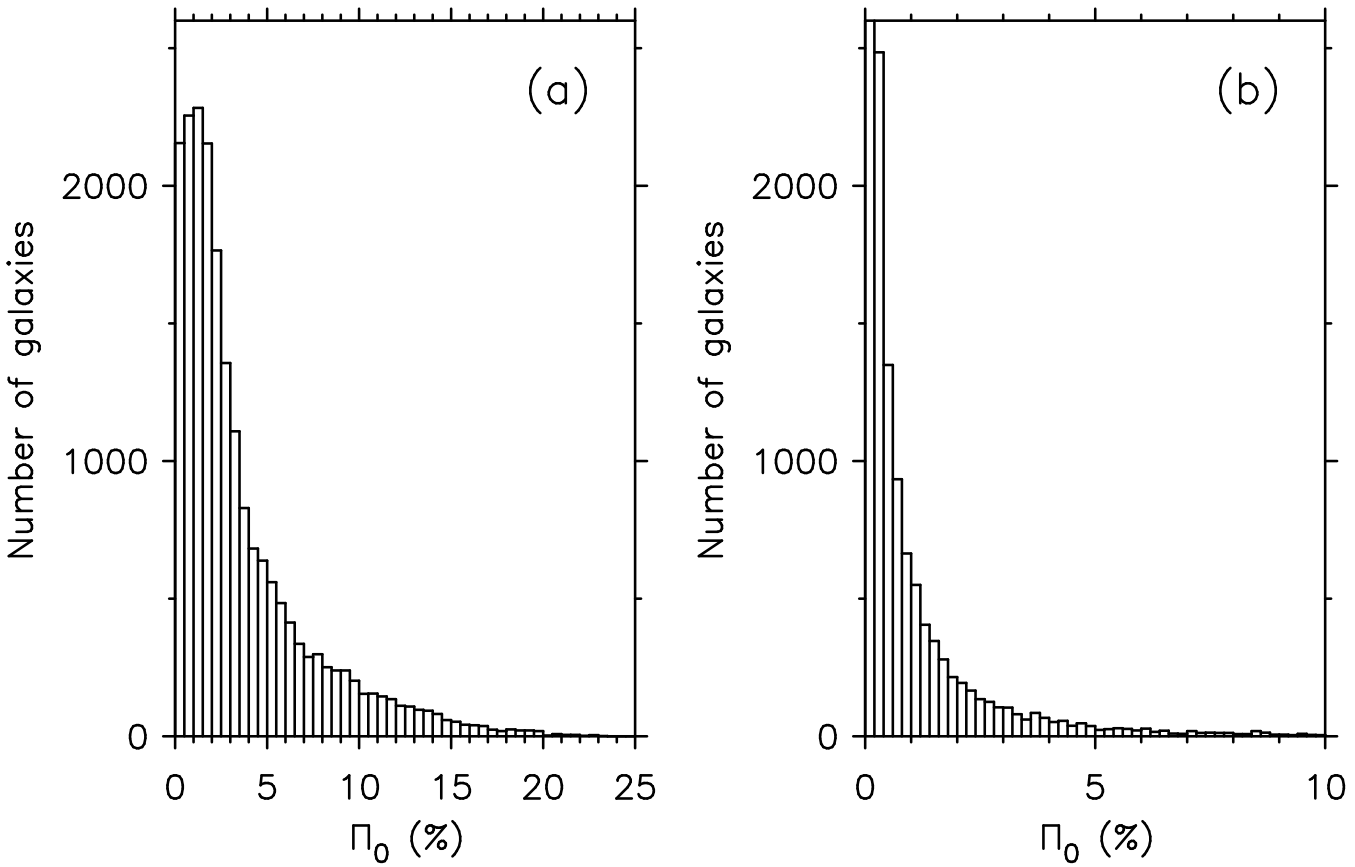

FIG. 6.— (a) Simulated histogram of fractional polarization of 20,000 randomly oriented model spiral galaxies at 4.8 GHz. Ranges of model parameters used for this simulation are given in Table 4. The fractional polarization for the same galaxies at 1.4 GHz is shown in (b). The vertical axis in (b) is truncated (lowest bin only).

wavelength and fitted to observations. Taylor et al. (2007) used Monte-Carlo simulations of noise statistics and observational selection effects, and derived the shape of the PDF for Π_0 for faint polarized sources from a maximum likelihood fit to the data. A similar approach can be used in the future to compare the PDF of Π_0 for galaxies at high redshift with the PDF for local galaxies.

The PDF for Π_0 follows from the probability $P(i)$ to observe a galaxy at inclination between i and $i + di$,

$$P(i)di = \sin(i)di \qquad (0^\circ \leq i \leq 90^\circ). \tag{4}$$

The probability to find a fractional polarization between Π_0 and $\Pi_0 + \Delta\Pi_0$ is equal to the probability to find a galaxy with inclination in one of up to two inclination ranges $i_{\rm min}$ to $i_{\rm max}$ that yield the same fractional polarization. Therefore,

$$P(\Pi_0)\Delta\Pi_0 = \sum_{k=1}^{N}(\cos i_{{\rm min},k} - \cos i_{{\rm max},k}) \tag{5}$$

In most cases, $N = 2$, except at the maximum of Π_0, where $N = 1$.

The PDFs of Π_0 for models 1 – 9 in Table 5 are shown in Figure 5. The median inclination for randomly-oriented galaxies is $i_{\rm med} = 60^\circ$. Nearly half (47%) of the galaxies in a randomly oriented set have inclination between 50° and 80°, for which Π_0 is near the maximum of the curves in Figure 1a. Consequently, all models predict a PDF that is sharply peaked toward the maximum possible value of Π_0.

Qualitatively, the shapes of the PDFs in Figure 5 do not depend strongly on the details of the models. The PDFs are derived from the curves in Figure 1. The shapes of these curves can be understood qualitatively in terms of two competing effects. If the inclination is not too large, the integrated polarization increases with inclination because of a larger net magnetic field in the plane of the sky. At higher inclinations, Faraday depolarization dominates and the integrated polarization decreases. A broad maximum in Π_0 must occur at intermediate inclination, that gives rise to the peak of the PDF near the maximum of Π_0.

Another feature of the PDFs in Figure 5 is that they converge to a constant value for small Π_0. The distribution is dominated here by galaxies at low inclination, with a smaller contribution of highly inclined galaxies with strong Faraday depolarization. Small fluctuations in the curves at small Π_0 are the result of occurrences where the Faraday rotation of the disk at the major axis is $\mathcal{R}\lambda^2 = n\pi$ ($n = 1, 2, 3, \ldots$) at high inclination. These fluctuations are small, and would not be noticed in observations.

The plateau in the distributions in Figure 5 can be understood based on a simple analytic argument. For inclination $i \lesssim 30^\circ$, the model curves in Figure 1 can be approximated with the relation $\Pi_0 = ai^2$, with the inclination i in radians and a a constant that depends on the model. The value of a may depend on complicated physics, but the only assumption here is that the increase of Π_0 for small i can approximated by a parabola, for

fixed parameters of the model. The probability to find a fractional polarization between Π_0 and $\Pi_0 + d\Pi_0$ is equal to the probability to find a galaxy with inclination in the interval $i_1 \leqq i \leqq i_2 < 30°$, with $\Pi_0 = a i^2_{\rm min,1}$, and $(\Pi_0 + d\Pi_0) = a i^2_{\rm max,1}$. Equation 5 reduces to

$$P(\Pi_0)d\Pi_0 = \cos i_{\rm min,1} - \cos i_{\rm max,1} = \frac{1}{2a}\Big(\frac{\sin i}{i}\Big)d\Pi_0. \quad (6)$$

The last step used that $(i_{\rm max,1} - i_{\rm min,1})$ is the infinitesimal increment $di = d\Pi_0/(2ai)$, and that $\frac{1}{2}(i_{\rm min,1} + i_{\rm max,1}) = i$. For $i < 30°$ the factor $\sin i/i \approx 1$ to an accuracy better than 5%, so $P(\Pi_0)$ is a constant that depends only on a. The models presented in Section 3 suggest that a depends mainly on the ratio of the random magnetic field to the regular magnetic field. This is why models 1, 2, and 3 converge to the same value for small Π_0, and models 4, 5, and 6 converge to a larger value. The differences between models 7, 8, and 9 arise from the more significant contributions from galaxies with a high inclination. These models also converge to a common value if only galaxies with low inclination are considered.

The distribution of Π_0 of an observed sample of spiral galaxies would be a superposition of a continuous set of model distributions similar to the nine curves in Figure 5. A simulated PDF for 20,000 galaxies with model parameters varied over the ranges given in Table 4 is shown in Figure 6. At 4.8 GHz (Figure 6a), the distribution of Π_0 is quite broad, with a peak between 1% and 2% polarization. The location of the peak and the depth of the minimum near $\Pi_0 = 0\%$ depends on the number of galaxies with strong Faraday depolarization. At 1.4 GHz (Figure 6b), Faraday depolarization is much stronger and the distribution is sharply peaked towards $\Pi_0 = 0\%$. For the distributions in Figure 6 we find that 78% of galaxies has $\Pi_0 > 1\%$ at 4.8 GHz, while at 1.4 GHz 17% has $\Pi_0 > 1\%$. The broad tail of the distribution in Figure 4b contains galaxies with low to moderate inclination. The median inclination for galaxies with $\Pi_0 > 5\%$ at 1.4 GHz is 41°.

Integrated polarimetry of an unbiased sample of a few hundred spiral galaxies would allow a statistical analysis for the Π_0 distributions of spiral galaxies, including subsets by inclination, morphological type and star formation rate. The Π_0 distribution can be retrieved from the data in the presence of noise through maximum likelihood fits presented by Taylor et al. (2007). The skewed shape on the PDF in Figure 6a, suggests that the best theoretical function to represent the PDF of spiral galaxies would be the lowest order *anti*-symmetric deviation from a Gaussian that shifts the peak of the distribution to a finite value of Π_0. In terms of the Gauss-Hermite series used in Taylor et al. (2007), the lowest order term would include coefficient h_3 (Van der Marel & Franx 1993).

4. DISCUSSION

4.1. *Diagnostics from integrated polarization*

We presented observations of the integrated polarization of nearby spiral galaxies to study the polarization properties of spiral galaxies as unresolved radio sources. It is shown that unresolved spiral galaxies are polarized radio sources with fractional polarization up to $\sim 20\%$ at 4.8 GHz. This high degree of fractional polarization arises from the regular azimuthal component of the magnetic field in the spiral galaxies observed, that is projected into a component in the plane of the sky that is predominantly oriented along the apparent major axis of the disk seen at inclination i. The projected magnetic field direction as implied by the plane of polarization, rotated by 90°, is well correlated with the position angle of the major axis for galaxies observed at higher inclination. The highest integrated polarization is expected for galaxies at intermediate inclination. For a sample of randomly oriented spiral galaxies, 47% has an inclination between 50° and 80°. Galaxies in this inclination range are under-represented in the present sample because the data used in this paper were obtained for polarization studies that preferred low-inclination or high-inclination galaxies. The number of galaxies with a high fractional polarization in Figure 1 may therefore be under represented compared with an unbiased sample.

Three of the eight Virgo spirals in our data set have integrated fractional polarization $\Pi_0 \geqq 8\%$. The range of Π_0 of the Virgo spirals is similar to that of the nearby "field" spirals. We do not find evidence in the present data that the integrated polarization of spiral galaxies in a cluster environment would be different from field galaxies. Although cluster galaxies are distorted by interactions with other galaxies and the intracluster medium (Weżgowiec et al. 2007; Chyży et al. 2007; Vollmer et al. 2007), the Virgo galaxies in our sample cannot be distinguished from field galaxies in their integrated polarization. This result should be verified with a larger, complete sample of cluster galaxies.

The barred galaxies in Table 3 show that a high integrated polarization also occurs for barred galaxies. In some of these barred galaxies, polarized emission from the bar is negligible compared to polarized emission from the disk. In other barred spirals, polarized emission from the bar region dominates, and the integrated polarization depends on the orientation of the bar, as well as the inclination of the galaxy. The effect of a bar is not included in the present models, so the existence of significant departures from the models is not unexpected. Non-axially symmetric models of the integrated polarization of spiral galaxies are deferred to a later paper.

Figure 3 suggests a difference between luminous and less luminous spiral galaxies. The three sub samples separately also show a smaller integrated fractional polarization for luminous spiral galaxies. Face-on galaxies and depolarized edge-on galaxies should exist at every luminosity, although they form a minority in a set of randomly oriented spiral galaxies. The presence of some galaxies with low Π_0 at every luminosity in Figure 3 is therefore not surprising. The luminous galaxies in the sample cover the same range in inclination as the galaxies with lower luminosity. This excludes selection effects in inclination as a possible origin of the correlation. No selection effect could be identified that would exclude luminous galaxies with a high Π_0 from the sample.

The lack of luminous galaxies with a high Π_0 gains significance in view of the results from Section 3.3. Given certain physical conditions, the inclination dependence of Π_0 favors high values of Π_0. The lower polarization of luminous spiral galaxies therefore indicates different conditions in these galaxies. A higher rate of star formation increases the random component of the magnetic field through the effect of supernova explosions and stel-

lar winds. A stronger total magnetic field and lower polarization are found locally in regions of galaxies where the star formation rate is high (Beck 2005; Chyży 2008). The correlation in Figure 3b may be explained similarly in terms of a generally higher star formation rate. The correlation of polarization with luminosity is an important factor for predictions of the number of spiral galaxies that will be detected in deep polarization surveys. Larger samples of spiral galaxies are required to confirm this result, and to allow more detailed modeling.

Simple axially symmetric models for the integrated polarization of spiral galaxies successfully describe the distribution of observed galaxies in the Π_0 - i diagram (Figure 1a). The results in Table 4 show that for $i \lesssim 50°$ the model is most sensitive to the parameter $f_{\rm B}$. This is so because wavelength-dependent depolarization such as Faraday dispersion and differential Faraday rotation are small compared with wavelength-independent depolarization in the models at 4.8 GHz with a small inclination. At higher inclination and at lower frequencies, wavelength-dependent depolarization is more important. A complete sample of spiral galaxies observed at 4.8 GHz may be divided into sub samples by inclination to separate the effects of different physical parameters. We discuss three inclination ranges.

Galaxies with inclination $i \lesssim 30°$ (13.4% of an unbiased sample) would display low fractional polarization, provided the galaxy is axially symmetric. Large-scale departures from axial symmetry likely result in a higher degree of polarization for these low-inclination galaxies. A statistical study of the integrated polarization of face-on spiral galaxies will therefore provide constraints on the large-scale asymmetry of polarized emission and therefore magnetic fields in spiral galaxies. For a sample of face-on barred galaxies, the orientation of the plane of polarization may be correlated with the position angle of the bar derived from optical images.

At inclinations $30° \lesssim i \lesssim 50°$ (22.3% of an unbiased sample), the axially symmetric models are most sensitive to the ratio of the random magnetic field to the regular magnetic field. This inclination range seems most promising to provide constraints of this parameter for a large sample of galaxies. Integrated polarimetry at more than one frequency may be combined to separate wavelength-dependent depolarization from wavelength-independent depolarization. More detailed models of the effect of non-axially symmetric structure such as spiral arms are required.

At inclinations $i \gtrsim 50°$ (64.3% of an unbiased sample), the longer path length and larger line-of-sight components of the regular magnetic field greatly enhance wavelength-dependent Faraday depolarization and Faraday rotation. This is confirmed by the results in Table 4, where the contribution of B, n_e, f_i, and $2h$ to the total scatter all rise to approximately equal amounts at inclination 75°. The ratio of random to regular magnetic field is still an important factor, but this can be constrained by results obtained from galaxies at lower inclination. Multi-frequency observations would be valuable because the models suggest that the strongest frequency dependence of depolarization of the integrated emission occurs for inclinations more than $\sim 60°$.

4.2. *Spiral galaxies as polarized background sources*

Are spiral galaxies suitable background sources for rotation measure studies? Internal Faraday rotation in distant spiral galaxies likely amounts to rotation measures of a few hundred rad m^{-2}. However, the correlation between $\theta_{\rm B}$ and $\theta_{\rm opt}$ in Figure 2a, and the models presented in Section 3 suggest that the plane of polarization is related to the orientation of the major axis of the optical disk. The polarization angle of an unresolved spiral galaxy is determined by the orientation of its major axis through the projection of the azimuthal magnetic field in the galactic disk on the plane of the sky. This is in part a result of the symmetry of the galaxies, as polarized emission from areas of the disk opposite to each other with respect to the center of the galaxy is Faraday rotated by equal but opposite angles. Depolarization resulting from differential Faraday rotation also mitigates the effect of Faraday rotation on the position angle of the integrated emission. The correlation in Figure 2a confirms that the plane of polarization is related to the orientation of the major axis in real galaxies.

The important implication is that the plane of polarization of a spiral galaxy that is unresolved by a radio telescope, is independent of wavelength. The orientation of the plane of polarization can be determined from the position angle of the optical major axis, although with a 180° ambiguity. As the plane of polarization does not depend on wavelength, we find the surprising result that *unresolved spiral galaxies behave as idealized polarized background sources without apparent internal Faraday rotation.* This result follows from axial symmetry. The 8.4 GHz polarization data in Table 2 seem to confirm that the polarization angle of the integrated emission is independent of wavelength. More observations are required to confirm this mainly theoretical result for more galaxies and at lower frequencies.

The intrinsic position angle of the plane of polarization of an unresolved spiral galaxy can be estimated from an optical image. It does not depend on internal Faraday rotation or on the spiral pitch angle of the magnetic field (Section 3). In principle, this property allows the detection of possible Faraday rotation by an intergalactic medium, using a large sample of spiral galaxies. The correlation between $\theta_{\rm B}$ and $\theta_{\rm opt}$ (Figure 2) can be made for a large number of galaxies, subdivided by distance and location in the sky. If large-scale magnetic fields exist in the nearby intergalactic medium, the correlation between $\theta_{\rm B}$ and $\theta_{\rm opt}$ would show an offset for more distant galaxies in a certain direction. The rotation measure sensitivity of such an experiment would depend primarily on the sample size of spiral galaxies with integrated polarimetry, and on the longest wavelength at which unresolved spiral galaxies remain polarized sources.

5. SUMMARY AND CONCLUSIONS

This paper discusses the integrated polarization properties of nearby galaxies from archival data at 4.8 GHz, and models for the integrated polarized emission of a spiral galaxy. We find that

1. Spiral galaxies can show substantially polarized (up to ∼20% at 4.8 GHz) integrated radio emission. The polarization angle of the integrated emission of spirals without a (strong) bar is aligned with the apparent minor axis of the disk. Barred spirals can also be polarized sources, but do not show a clear correlation of polariza-

tion angle with the orientation of the major axis.

2. The highest degree of polarization, and the largest spread in fractional polarization, are found for spiral galaxies with intermediate to high inclination ($i \gtrsim 50°$).

3. A sub-sample of nine spiral galaxies in the Virgo cluster does not show a significant difference in integrated polarization properties from the field galaxies in our sample. This suggests that physical distortions of these galaxies are not so strong that they have a noticeable effect on the integrated polarization. Confirmation by a larger, complete sample is required.

4. The fractional polarization of integrated emission is smaller for galaxies with a higher radio luminosity. This result suggests a difference in properties of the magnetic field and/or Faraday depolarization in luminous spiral galaxies.

5. Our models for the integrated polarization of axially symmetric spiral galaxies cover the same area in the Π_0-i diagram (Figure 1) as the observed galaxies without a strong bar. The models indicate that the main cause of variation in the fractional polarization of galaxies with inclination less than 50° is the ratio of the random to the regular magnetic field component in the disk.

6. Our models provide a probability density function of fractional polarization of spiral galaxies as a function of wavelength that can be used to predict the number of spiral galaxies in deep polarization surveys, and to study the statistical properties of spiral galaxies in such surveys.

7. The integrated polarization of spiral galaxies opens the possibility to study magnetic field properties and Faraday rotation in large samples of spiral galaxies, and in galaxies at high redshift. A deep 1 - 2 GHz survey with the SKA could detect normal spiral galaxies at redshift 1 or higher (Wilman et al. 2008) with a total intensity flux ~ 100 μJy. These can be compared in a resolution-independent way with integrated polarization measurements of low-redshift galaxies at the same rest-frame frequency.

8. Unresolved symmetric spiral galaxies behave as idealized background sources without internal Faraday rotation. They can be used to detect large-scale magnetic fields in the intergalactic medium, e.g. with the SKA (Gaensler et al. 2004; Stepanov et al. 2008).

We thank Marek Weżgowiec and Marek Urbanik for giving us the maps of the Virgo galaxies, some of them prior to publication. The authors thank K. T. Chyży for the use of data for NGC 4254 and NGC 4736. We also acknowledge Maike Lensing for her help to prepare the radio maps for the flux integration. The authors thank the referee for comments that helped to improve the manuscript. This research has made use of the NASA/IPAC Extragalactic Database (NED) which is operated by the Jet Propulsion Laboratory, California Institute of Technology, under contract with the National Aeronautics and Space Administration.

REFERENCES

Arshakian, T., Stepanov, R., Beck, R., Frick, P., & Krause, M. 2007, arXiv:0711.4979
Beck, R., Krause, M., & Klein, U. 1985, A&A, 152, 237
Beck, R., & Hoernes, P. 1996, Nature, 379, 47
Beck, R., Shoutenkov, V., Ehle, M., Harnett, J. I., Haynes, R. F., Shukurov, A., Sokoloff, D. D., Thierbach, M. 2002, A&A, 391, 83
Beck, R. 2005, in Cosmic Magnetic Fields, ed. R. Wielebinski & R. Beck (Heidelberg:Springer), 41
Beck, R. 2007, EAS Publ. Ser., 23, 19
Beck, R. 2007, A&A, 470, 539
Berkhuijsen, E. M., Beck, R., & Hoernes, P 2003, A&A, 398, 937
Binney, J. & de Vaucouleurs, G. 1981, MNRAS, 194, 679
Brown, J. C., Taylor, A. R., Wielebinski, R., & Mueller, P. 2003, ApJ592, L29
Brown, J. C., Haverkorn, M., Gaensler, B. M., Taylor, A. R., Bizunok, N. S., McClure-Griffiths, N. M., Dickey, J. M., & Green, A. J. 2007, ApJ663, 258
Burn, B. J. 1966, MNRAS, 133, 67
Chyży, K. T., Ehle, M., & Beck, R. 2007, A&A, 474, 415
Chyży, K. T. 2008, A&A, 482, 755
Chyży, K. T., & Buta, R.J. 2008, ApJ, 677, L17
Condon, J. J. & Yin, Q. F. 1990, ApJ, 357, 97
Condon, J. J. 1992, ARA&A, 30, 575
Dumke, M., & Krause, M., 1998, Lecture Notes in Physics, 506, 555
Dumke, M., Krause, M., & Wielebinski, R. 2000, A&A, 355, 512
Fletcher, A., Beck, R., Berkhuijsen, E. M., Horellou, C., Shukurov, A. 2004, in How does the Galaxy work?, ed. E. J. Alfaro et al. (Dordrecht: Kluwer), 299
Gaensler, B., Beck, R., & Feretti, L. 2004, New Ast. Rev., 48, 1003
Gaensler, B., Haverkorn, M., Staveley-Smith, L., Dickey, J. M., McClure-Griffith, N. M., Dickel, J. R., & Wolleben, M. 2005, Science, 307, 1610
Golla, G., & Hummel, E. 1994, A&A, 284, 777
Gräve, R., & Beck, R. 1988, A&A, 192, 66
Grosbøl, P. J. 1985, A&AS, 60, 261
Han, J. L., Beck, R., Berkhuijsen, E. M. 1998, A&A, 335, 1117
Han, J. L., Manchester, R. N., Qiao, G. J. 1999, MNRAS, 306, 371
Heesen, V., Dettmar, R.-J., Kause, M., & Beck, R. 2008, PoS(MRU)089 arXiv:0801.3542
Johnston, S., et al. 2007, PASA, 24, 174
Krause, M. 2003, in The Magnetized Interstellar Medium, Proceedings of the conference, held in Antalya, Turkey, September 8 - 12, 2003, Ed. B. Uyaniker, W. Reich, and R. Wielebinski, Copernicus GmbH, Katlenburg-Lindau., 173
Lambas, D. G., Maddox, S. J., & Loveday, J. 1992, MNRAS, 258, 404
Niklas, S., Klein, U., Wielebinski, R. 1997, A&A, 322, 19
Simmons, J. F. L., & Stewart, B. G. 1985, A&A, 142, 100
Sokoloff, D. D., Bykov, A. A., Shukurov, A., Berkhuijsen, E. M., Beck, R., & Poezd, A. D. 1998, MNRAS, 299, 189
Spangler, S. R. 1982, ApJ, 261, 310
Stil, J. M., Taylor, A. R., Krause, M., & Beck, R. 2007, PoS(MRU)069 arXiv:0802.1374
Stepanov, R., Arshakian, T. G., Beck, R., Frick, P., & Krause, M. 2008, A&A, 480, 45
Tabatabaei, F. S., Krause, M., & Beck, R. 2007, A&A, 472, 785
Tüllmann, R., Dettmar, R.-J., Soida, M., Urbanik, M., Rossa, J. 2000, A&A, 364, L36
Taylor, A. R., et al. 2007, ApJ, 666, 201
Van der Marel, R. P., & Franx, M. 1993, ApJ, 407, 525
Vollmer, B., Soida, M., Beck, R., Urbanik, M., Chyży, K. T., Otmianowska-Mazur, K., Kenney, J. D. P., Van Gorkom, J. H. 2007, A&A, 464, L37
Weżgowiec, M., Urbanik, M., Vollmer, B., Beck, R., Chyży, K. T., Soida, M., & Balkowski, Ch. 2007, A&A, 471, 93
Wilman, R. J., Miller, L., Jarvis, M. J., Mauch, T., Levrier, F., Abdala, F. B., Rawlings, S., Klöckner, H.-R., Obreschkow, D., Olteanu, D. & Young, S. 2008, MNRAS, 388, 1335